A Novel Four-Quadrant Propeller Model

Andreas J. Häusler[1], Alessandro Saccon[2], John Hauser[3], António M. Pascoal[1], and A. Pedro Aguiar[4]

[1] Laboratory of Robotics and Systems in Science and Engineering, Instituto Superior Técnico, Lisbon, Portugal

[2] Eindhoven University of Technology, Eindhoven, The Netherlands

[3] Electrical, Computer, and Energy Engineering Department, University of Colorado at Boulder, Boulder, Colorado, USA

[4] Faculdade de Engenharia, University of Porto, Porto, Portugal

ABSTRACT

Autonomous marine vehicles (AMVs) are small-scale surface and underwater robots that execute maneuvers where the thrusters operate in all four quadrants of motion: ahead, crash-back, back, and crash-ahead. This is typically the case if vehicle steering is done using differential thrusting instead of deflecting control planes. Existing quasi-steady four-quadrant propeller models can properly describe the phenomena apparent in each of the quadrants, but suffer from computational difficulties if thrust and torque have to be evaluated often as, e.g., in simulations.

In this work, we briefly review a quasi-steady four-quadrant propeller model that we previously developed to overcome these difficulties, and elaborate its performance in comparison with two other models. To that avail, we also show an ideal propeller model based on momentum theory, that has been extended to be applicable in all four quadrants of motion.

Keywords

Four Quadrant Propeller Modeling, Momentum Theory, Propeller Efficiency, Quasi-Steady Propeller Model.

1 INTRODUCTION

In order to lay the ground for the discussion in this paper, we review classical propeller models (open-water and four-quadrant) as well as an existing approximation to the four-quadrant model in Section 1. Section 2 introduces a low-order harmonic approximation of the standard four-quadrant model, and we develop an ideal model valid for all four quadrants in Section 3. In Section 4, we discuss and compare energy related features of all propeller models presented here, and conclude the paper with an outlook to future research in Section 5.

1.1 Classical Propeller Models

The most common approach to modeling a marine vehicle's propeller-driven thruster system is by means of static equations for propeller thrust and torque. Several different static equation systems exist in the literature; yet, to the best of the authors' knowledge, the choice that dominates by far is the so-called *open-water propeller model*, in which propeller thrust T and torque Q are described in terms of the open-water coefficients $k_{\mathrm{T}}(J_{\mathrm{o}})$ and $k_{\mathrm{Q}}(J_{\mathrm{o}})$, respectively, as

$$T = \rho d^4 k_{\mathrm{T}}(J_{\mathrm{o}}) n|n| \tag{1a}$$

$$Q = \rho d^5 k_{\mathrm{Q}}(J_{\mathrm{o}}) n|n|\,, \tag{1b}$$

where ρ is the density of the surrounding water, d is the propeller rotor diameter, and n is the rotational velocity of the propeller. (For further details, the reader is referred to (Fossen, 2002, Sec. 12.2) or (Smogeli, 2006, Sec. 2.1).) The inherent problem with the propeller model (1) lies in the fact that the open-water thrust and torque coefficients k_{T} and k_{Q} are defined in terms of the open-water advance ratio

$$J_{\mathrm{o}} := \frac{v_{\mathrm{a}}}{nd}\,, \tag{2}$$

where v_{a} is the propeller's (and the vessel's) advance speed as above. Clearly, a zero-crossing of the propeller speed n makes the advance ratio (2) go to infinity. This naturally invalidates the modeling of propeller movements outside the limitation to forward oriented thrust along with a forward motion through the water.

In their seminal publication, van Lammeren et al. (1969) describe the *four-quadrant propeller model*, which is valid for operations in all quadrants of motion, rendering it suitable to avoid the aforementioned problem. The model, from here on called the **W**-model in reference to the *Wageningen propeller series*, defines propeller thrust and torque as

$$T = \frac{1}{2}\rho c_{\mathrm{T}}^{\mathbf{W}}(\beta)\big(v_{\mathrm{a}}^2 + v_{\mathrm{p}}^2\big)\pi R^2 \tag{3a}$$

$$Q = \frac{1}{2}\rho c_{\mathrm{Q}}^{\mathbf{W}}(\beta)\big(v_{\mathrm{a}}^2 + v_{\mathrm{p}}^2\big)\pi R^2 d\,, \tag{3b}$$

where R and $d = 2R$ are the propeller radius and diameter, respectively, v_{a} is the ambient water velocity, and $v_{\mathrm{p}} = 0.7R\omega$ is the tangential velocity of a propeller blade at a distance of $0.7R$ from the propeller axis. The four-quadrant thrust and torque coefficients, $c_{\mathrm{T}}^{\mathbf{W}}(\beta)$ and $c_{\mathrm{Q}}^{\mathbf{W}}(\beta)$ are given in terms of the advance angle β at the the propeller blade. This angle, given as $\beta = \operatorname{atan2}(v_{\mathrm{a}}, v_{\mathrm{p}})$ for right-rotating and as $\beta = \pi - \operatorname{atan2}(v_{\mathrm{a}}, v_{\mathrm{p}})$ for left-rotating propellers, defines the four quadrants of operation. An illustration of β and related kinematic and dynamic quantities is given in Figure 1 for

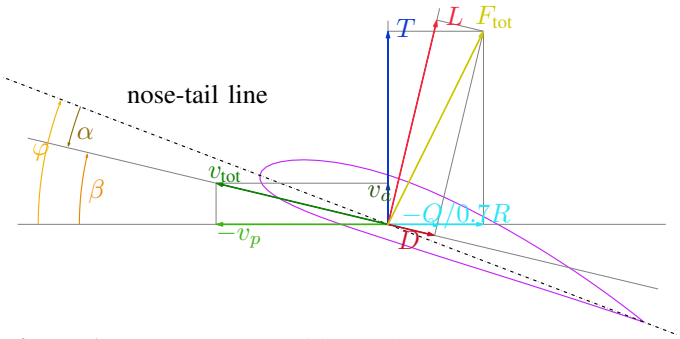

Figure 1: Forces and velocities acting on a propeller blade.

the case of a propeller that is left-rotating for forward-thrust generation (the propeller is moving vertically upwards in this picture, while the propeller blade, whose contour is shown in the figure, is moving to the left). In van Lammeren et al. (1969) and Oosterveld (1970), measurement-based values for $c_{\text{T}}^{\textbf{W}}(\beta)$ and $c_{\text{Q}}^{\textbf{W}}(\beta)$ are given as 20th order Fourier series for a selection of propeller/nozzle combinations.

1.2 The Approximation by Healey et al.

Our work on motion planning (Häusler et al., 2012) for multiple AMVs defines trajectory generation as an optimization problem explicitly incorporating the vehicle model as well as a model of the full propulsion system, including (3). In the solution of this class of problems, the **W**-model exhibits numerical issues related to the highly non-convex nature of $c_{\text{T}}^{\textbf{W}}(\beta)$ and $c_{\text{Q}}^{\textbf{W}}(\beta)$, where a Newton optimization method for trajectory generation that involves the propeller model would not be able to find a second order descent direction. An interesting approximation of the **W**-model has been presented in Healey et al. (1995)—in the remainder of this paper, we refer to it as the **H**-model. Instead of working directly with thrust T and torque Q, the **H**-model solves the approximation in the lift-and-drag frame: lift L and drag D are defined in terms of the sinusoidal lift and drag coefficients

$$c_{\text{L}}^{\textbf{H}}(\alpha) = c_{\text{L}_{\text{max}}} \sin(2\alpha) \tag{4a}$$

$$c_{\text{D}}^{\textbf{H}}(\alpha) = c_{\text{D}_{\text{max}}} (1 - \cos 2\alpha)/2\,, \tag{4b}$$

where $\alpha = \varphi - \beta$ is the angle of attack at the propeller blade, and φ is the (constant) propeller pitch angle (Carlton, 2007, Figure 3.4). Since thrust and torque forces at the propeller blade are related to lift and drag by a simple rotation about β, the **H**-model replaces the Fourier series based thrust and torque coefficients of the **W**-model in (3) by

$$c_{\text{T}}^{\textbf{H}}(\beta) = \quad c_{\text{L}}^{\textbf{H}}(\beta)\cos(\beta) - c_{\text{D}}^{\textbf{H}}(\beta)\sin(\beta) \tag{5a}$$

$$c_{\text{Q}}^{\textbf{H}}(\beta) = \frac{0.7}{2}\big(c_{\text{L}}^{\textbf{H}}(\beta)\sin(\beta) + c_{\text{D}}^{\textbf{H}}(\beta)\cos(\beta)\big)\,, \tag{5b}$$

which is an approximation of $c_{\text{T}}^{\textbf{W}}(\beta)$ and $c_{\text{Q}}^{\textbf{W}}(\beta)$. We discovered, however, that the **H**-model does not exhibit certain physical key properties (Häusler et al., 2013):

- The **H**-model coefficients (5) are 0 for the same advance angle, causing T and Q to go through 0 at the same advance angle. Physics, however, suggests that the thrust must to go to 0 slightly *before* the torque reaches 0 (cf. (Fossen, 2002, Figure 12.2), van Lammeren et al. (1969), or (Oosterveld, 1970, Figure 37)).
- Drag should attain its minimum at a slightly positive lift (see e.g. (Carlton, 2007, Figure 7.2) or Sheldal and Kilmee (1981)). In the **H**-model, both are 0 at the same angle of attack.
- The minimum of $c_{\text{D}}(\alpha)$ should be non-negative because of a *residual drag* component that is missing in the **H**-model (Figure 2)—see the important remarks in (Anderson, 1999, p. 132), illustrated by the drag polar diagrams in (Abbott and von Doenhoff, 1959, Chapter 7).

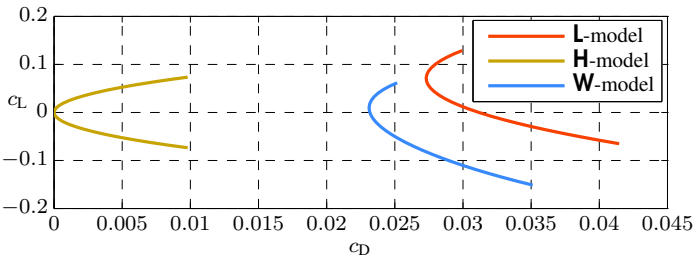

Figure 2: Drag polars for the different four-quadrant models.

2 LOW-ORDER HARMONIC APPROXIMATION

In Häusler et al. (2013), we proposed the **L**-model as a modification of (4), which we showed to be (a) conform to propeller theory, (b) close to the **W**-model in the main region of operation in terms of β, and (c) exhibiting certain monotonicity properties that are advantageous when dealing with numerical optimization. Using a passivity-based argument on the efficiency of the propeller, we also demonstrated that the proposed model avoids the efficiency related issues present in the **H**-model. Due to space limitations, we restrict ourselves to the definition of the **L**-model; the reader is referred to Häusler et al. (2013) for further details.

The **L**-model of a propeller is defined through the relations

$$c_{\text{L}}^{\textbf{L}}(\alpha) = c_{\text{L}}^{\text{max}} \sin 2(\alpha - o_{\text{L}}) \tag{6a}$$

$$c_{\text{D}}^{\textbf{L}}(\alpha) = \big(c_{\text{D}}^{\text{max}} - c_{\text{D}}^{\text{min}}\big)\big(1 - \cos 2(\alpha - o_{\text{D}})\big)/2 + c_{\text{D}}^{\text{min}}\,, \tag{6b}$$

where (6a) and (6b) are intended to replace (4a) and (4b), respectively. The five parameters ($c_{\text{L}}^{\text{max}}$, $c_{\text{D}}^{\text{min}}$, $c_{\text{D}}^{\text{max}}$, o_{L}, and o_{D}) in the **L**-model (6) can be obtained by solving a nonlinear least

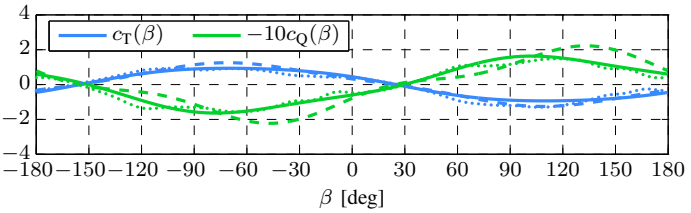

Figure 3: Four-quadrant thrust and torque coefficients: **W**-model (dotted), **H**-model (dashed), and **L**-model (solid).

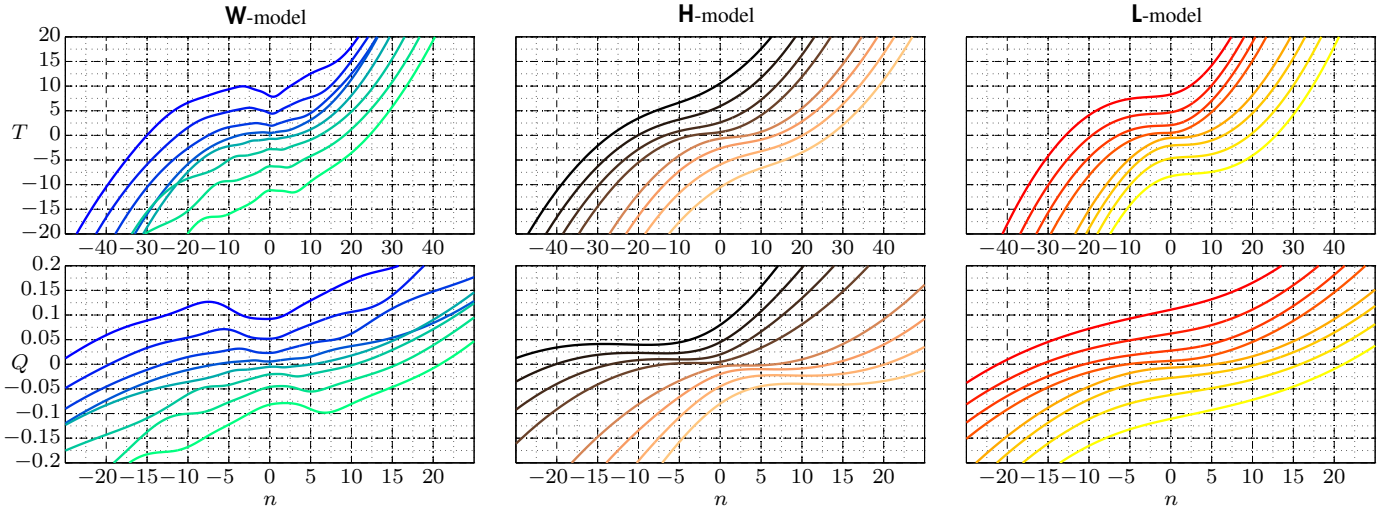

Figure 4: A comparison of thrust T and torque Q produced by the three different propeller models under consideration. The colors indicate the value of the advance velocity v_a, ranging from $-2\frac{\mathrm{m}}{\mathrm{s}}$ (light colors) to $2\frac{\mathrm{m}}{\mathrm{s}}$ (dark colors) with an interval of $0.5\frac{\mathrm{m}}{\mathrm{s}}$.

squares problem that seeks to capture characteristics of first quadrant open-water efficiency of the **W**-model while fitting the $c_\mathrm{T}^\mathbf{W}(\beta)$ and $c_\mathrm{Q}^\mathbf{W}(\beta)$ curves in the primary operating region $0° \leq \beta \leq 50°$ (Figure 3). We have also enforced a monotonicity constraint on the level curves of the produced thrust (Figure 4, rightmost plot). Numerical values of the parameters in (6) were found to be $o_\mathrm{L} = -1.6157°$, $o_\mathrm{D} = 1.9309°$, $c_\mathrm{D}^\mathrm{min} = 0.0273$, $c_\mathrm{L}^\mathrm{max} = 0.5749$, and $c_\mathrm{D}^\mathrm{max} = 1.0383$. With the obtained values of $o_\mathrm{L} \neq o_\mathrm{D}$, we found that the minimum drag is indeed obtained at a slightly positive lift, which is in line with what is common for real airfoils (Anderson, 1999)—see also the drag polar diagram shown in Figure 2.

3 THE PROPELLER MODEL AS OBTAINED FROM MOMENTUM THEORY

The four-quadrant model, mainly due to its relative complexity, is—despite being often reviewed in the literature—seldom used at the application level. On this account, we now develop a *momentum theory* based propeller model that reflects a much more widely used approach. By comparing the results obtained with the various propeller models, we can judge whether the level of detail provided by the **W**-model is needed for our purpose, i.e., the generation of energy minimal trajectories in the optimal control based optimization framework published by Hauser (2002). The discussion presented here is closely leaned towards the helicopter theory books by Leishman (2006), by Johnson (1994), and by Seddon (1990), which have been used as main resources.

The core idea in momentum theory is to view the propeller as *actuator disk*, i.e., the propeller is assumed to have an infinite number of blades, which are further assumed to have zero thickness. A picture of the general set-up on which the discussion is based is given in Figure 5a. The physics of the propeller behavior are formulated by application of Bernoulli's law, which makes the assumptions that (a) the

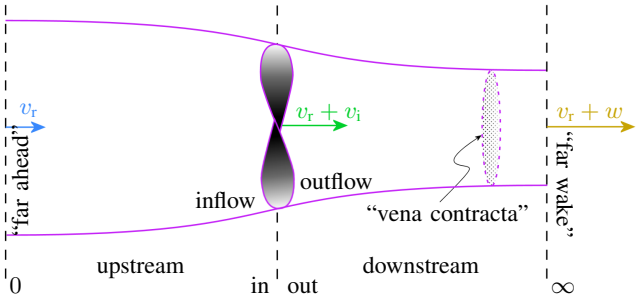

a: Stream tube created by a propeller moving from left to right.

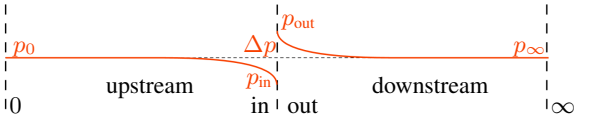

b: Pressure in the flow as a function of distance to the actuator disk.

Figure 5: The stream tube created by a propeller.

flow is incompressible, (b) the propeller is moving in an ideal fluid, i.e. the viscous friction is negligible, and (c) there is no rotational flow. For part of this discussion, it is essential to keep in mind the pressure in the flow as a function of the distance to the actuator disk, as shown in Figure 5b, which especially highlights the discontinuity of the pressure at the disk, a result of the simplifying assumption that the disk has no width.

In what follows, the subscripts $_0$, $_\mathrm{in}$, $_\mathrm{out}$, and $_\infty$ refer to the four "stations" in Figures 5a and 5b. This illustration shows a propeller that is rotating in such a way that the whole vehicle (not shown) moves to the left, i.e., the inflowing water comes from the left. We assume a left-rotating (as seen from behind the vessel) propeller moving in direction of the viewer on top and into the paper on the bottom.

3.1 Development for Positive Thrust

We begin the presentation limited to thrust $T > 0$, i.e., we only consider induced velocity $v_\mathrm{i} > 0$. (The *induced velocity* is the velocity imparted to the mass of water contained in the control volume at the rotor disk (Leishman, 2006, p. 61).)

A)Zero relative velocity: Consider first the relative velocity of the water as zero, $v_\mathrm{r} = 0\frac{\mathrm{m}}{\mathrm{s}}$. The discontinuity in the pressure (Figure 5b) requires Bernoulli's law (the sum of static and dynamic pressure being constant at each point in the same control volume) to be expressed with two equations:

$$p_0 + \frac{1}{2}\rho v_\mathrm{r}^2 = p_\mathrm{in} + \frac{1}{2}\rho(v_\mathrm{r} + v_\mathrm{i})^2 \qquad \text{inflow} \qquad (7)$$

$$p_\mathrm{out} + \frac{1}{2}\rho(v_\mathrm{r} + v_\mathrm{i})^2 = p_\infty + \frac{1}{2}\rho(v_\mathrm{r} + w)^2 \qquad \text{outflow} \qquad (8)$$

With $v_\mathrm{r} = 0$, the difference in pressure is

$$\Delta p = p_\mathrm{out} - p_\mathrm{in} = p_\infty + \frac{1}{2}\rho w^2 - p_0 = \frac{1}{2}\rho w^2\,, \qquad (9)$$

since the ambient pressure does not change, i.e. $p_0 = p_\infty$. By assumption, Δp is uniform across the propeller disk and must thus be equal to the *disk loading*, defined through the produced thrust T and the area of a cross-section of the stream tube at the propeller disk A_p as

$$\Delta p = \frac{T}{A_\mathrm{p}}\,. \qquad (10)$$

The law of *momentum conservation* for fluids tells us that $T = (\dot{m}v)_\mathrm{downstream} - (\dot{m}v)_\mathrm{upstream}$ with $\dot{m}$ as the mass flow of the water and v some general velocity of the water. In our case, this means that

$$T = \dot{m}w - \dot{m}0\,, \qquad (11)$$

since $v_\mathrm{r} = 0\frac{\mathrm{m}}{\mathrm{s}}$. By the *mass conservation* law, we know that

$$\dot{m} = \rho A_\mathrm{p} v_{\mathrm{i}_0} = \rho A_\infty w\,, \qquad (12)$$

where A_∞ is the far wake area of the stream tube and v_{i_0} is the induced velocity at $v_\mathrm{r} = 0\frac{\mathrm{m}}{\mathrm{s}}$. Thus, the thrust produced is $T = \dot{m}w = \rho A_\mathrm{p} v_{\mathrm{i}_0} w$ or, in other words,

$$\frac{T}{A_\mathrm{p}} = \rho v_{\mathrm{i}_0} w\,. \qquad (13)$$

With (9), we get

$$\Delta p = \frac{1}{2}\rho w^2 = \rho v_{\mathrm{i}_0} w = \frac{T}{A_\mathrm{p}}\,, \qquad (14)$$

which gives us the important result that half of the flow acceleration takes place "before" the disk and the other half "after" (see e.g. Carlton (2007); Leishman (2006)):

$$\boxed{v_{\mathrm{i}_0} = \frac{1}{2}w\,.} \qquad (15)$$

Using this result, thrust can also be written as

$$T = \dot{m}w = 2\dot{m}v_{\mathrm{i}_0} = 2\rho A_\mathrm{p} v_{\mathrm{i}_0}^2\,, \qquad (16)$$

which gives us another equation for the induced velocity at zero relative water velocity:

$$\boxed{v_{\mathrm{i}_0} = \sqrt{\frac{T}{2\rho A}} = \sqrt{T_\mathrm{n}}\,,} \qquad (17)$$

where $A = A_\mathrm{p}$ is the area of the propeller disk and T_n is the "normalized thrust". Finally, the power required at $v_\mathrm{r} = 0\frac{\mathrm{m}}{\mathrm{s}}$ is the "ideal power" (Leishman, 2006, p. 63)

$$P = T v_{\mathrm{i}_0} = T\sqrt{T_\mathrm{n}} = T^{3/2}/\sqrt{2\rho A} \qquad (18)$$

or

$$\boxed{P = T v_{\mathrm{i}_0} = 2\dot{m}v_{\mathrm{i}_0}^2 = 2\rho A v_{\mathrm{i}_0}^3\,.} \qquad (19)$$

B)Forward movement: In forward movement, the relative velocity of the water is $v_\mathrm{r} > 0$. As before, Bernoulli's law cannot be formulated as a single expression, resulting in

$$p_0 + \frac{1}{2}\rho v_\mathrm{r}^2 = p_\mathrm{in} + \frac{1}{2}\rho(v_\mathrm{r} + v_\mathrm{i})^2 \qquad \text{inflow} \qquad (20)$$

$$p_\mathrm{out} + \frac{1}{2}\rho(v_\mathrm{r} + v_\mathrm{i})^2 = p_\infty + \frac{1}{2}\rho(v_\mathrm{r} + w)^2 \qquad \text{outflow} \qquad (21)$$

Again, by conservation of fluid momentum, we get

$$T = \dot{m}(v_\mathrm{r} + m) - \dot{m}v_\mathrm{r} = \dot{m}w\,, \qquad (22)$$

which is, with mass conservation (i.e. $\dot{m} = \rho A_\mathrm{p}(v_\mathrm{r} + v_\mathrm{i})$),

$$T = \rho A_\mathrm{p}(v_\mathrm{r} + v_\mathrm{i})w\,. \qquad (23)$$

With $p_0 = p_\infty$, the pressure difference at the actuator disk is

$$\Delta p = p_\mathrm{out} - p_\mathrm{in} = \rho v_\mathrm{r} w + \frac{1}{2}\rho w^2 = \frac{1}{2}\rho(2v_\mathrm{r} + w)w \qquad (24)$$

and also (disk loading)

$$\Delta p = \frac{T}{A_\mathrm{p}} = \frac{\dot{m}w}{A_\mathrm{p}} = \rho(v_\mathrm{r} + v_\mathrm{i})w\,. \qquad (25)$$

With (24) and (25) we get

$$v_\mathrm{i} = \frac{1}{2}w\,, \qquad (26)$$

which proofs that (15) also holds for non-zero, positive relative water velocity v_r. Again using the fact that the area of the stream tube section at the actuator disk is equal to the area of the propeller disk, $A = A_\mathrm{p}$, we thus can conclude that

$$T = 2\rho A(v_\mathrm{r} + v_\mathrm{i})v_\mathrm{i}\,. \qquad (27)$$

We know from (16) that

$$\frac{T}{2\rho A} = v_{\mathrm{i}_0}^2\,, \qquad (28)$$

and with (27) we get

$$\left(\frac{v_\mathrm{i}}{v_{\mathrm{i}_0}}\right)^2 + \frac{v_\mathrm{r}}{v_{\mathrm{i}_0}}\left(\frac{v_\mathrm{i}}{v_{\mathrm{i}_0}}\right) - 1 = 0\,, \qquad (29)$$

the solution of which gives us a function describing the induced velocity variation for positive relative water velocity

in terms of v_r and v_{i_0} (Leishman, 2006, Section 2.13):

$$\boxed{\left(\frac{v_\mathrm{i}}{v_{\mathrm{i}_0}}\right) = -\left(\frac{v_\mathrm{r}}{2v_{\mathrm{i}_0}}\right) \pm \sqrt{\left(\frac{v_\mathrm{r}}{2v_{\mathrm{i}_0}}\right)^2 + 1}\,.} \tag{30}$$

Since, in forward motion, it must hold that $v_\mathrm{i}/v_{\mathrm{i}_0} > 0$, only the summation is leading to a valid expression in (30). Moreover, by basic physics,

$$\boxed{P = T(v_\mathrm{r} + v_\mathrm{i})\,.} \tag{31}$$

According to (Seddon, 1990, p. 10), Tv_r in this expression is the work done on the rotor, while Tv_i is the work done on the fluid, represented by the kinetic energy in the induced velocity. Stating that

$$v_\mathrm{i} = \left(\frac{v_\mathrm{i}}{v_{\mathrm{i}_0}}\right) v_{\mathrm{i}_0}\,, \tag{32}$$

we see that we may use the function (30) when computing (31) for our propeller.

C)In the crash-ahead regime: In crash-ahead, the flow is coming from the back of the vehicle, i.e., it is moving backwards while the propeller rotates in forward drive. In terms of the four-quadrant model, we are in the fourth quadrant; $v_\mathrm{r} < 0$ and $T > 0$. The pressure equations now change to

$$p_0 + \frac{1}{2}\rho(v_\mathrm{r} + w)^2 = p_\mathrm{in} + \frac{1}{2}\rho(v_\mathrm{r} + v_\mathrm{i})^2 \qquad \text{inflow} \tag{33}$$

$$p_\mathrm{out} + \frac{1}{2}\rho(v_\mathrm{r} + v_\mathrm{i})^2 = p_\infty + \frac{1}{2}\rho v_\mathrm{r}^2\,, \qquad \text{outflow} \tag{34}$$

and again with $\Delta p = p_\mathrm{in} - p_\mathrm{out}$, we get

$$\Delta p = \frac{1}{2}\rho(2v_\mathrm{r} + w)w \tag{35}$$

In contrast to (22), momentum conservation now tells us that

$$T = \dot{m}v_\mathrm{r} - \dot{m}(v_\mathrm{r} + w) = -\dot{m}w = -\rho A_\mathrm{p}(v_\mathrm{r} + v_\mathrm{i})w\,, \tag{36}$$

where we used the mass conservation law to obtain the last line. Again, with the disk loading $\Delta p = T/A_\mathrm{p}$, we get

$$v_\mathrm{i} = \frac{1}{2}w\,, \tag{37}$$

which now makes this expression true for all v_r and positive T. With (36) and (37), as well as $A = A_\mathrm{p}$, we thus obtain

$$T = -2\rho A(v_\mathrm{r} + v_\mathrm{i})v_\mathrm{i} \tag{38}$$

and finally

$$v_{\mathrm{i}_0}^2 = -(v_\mathrm{r} + v_\mathrm{i})v_\mathrm{i}\,. \tag{39}$$

We get an equivalent expression to (30) for negative v_r,

$$\boxed{\left(\frac{v_\mathrm{i}}{v_{\mathrm{i}_0}}\right) = -\left(\frac{v_\mathrm{r}}{2v_{\mathrm{i}_0}}\right) \pm \sqrt{\left(\frac{v_\mathrm{r}}{2v_{\mathrm{i}_0}}\right)^2 - 1}} \tag{40}$$

and this time subtraction is the only valid option, since $v_\mathrm{i}/v_{\mathrm{i}_0} > 0$ must hold. The instantaneous power requirement to generate T with a given v_r is, in this case, also expressible as in (31), while keeping in mind that the numeric value will be different since $v_\mathrm{r} < 0$.

3.2 Negative Thrust and Model Summary

Negative thrust occurs in the second (crash-back: $v_\mathrm{r} > 0$, $T < 0$) and third (backward motion: $v_\mathrm{r} < 0$, $T < 0$) quadrant, and is usually not considered in momentum theory discussions. For the reasons previously elaborated (cf. Section 2), however, we are interested in extending the existing work to four quadrants. Since momentum theory considerations do not take into account any information about the construction of the propeller, we assume symmetry in the thrust and torque generated for positive and negative rotational speed. In other words, we want the third quadrant (backward motion) to "behave" in the same way as the first quadrant, and the second quadrant (crash-back) as the fourth. Assuming this kind of symmetry, it must hold that

$$T > 0 \Rightarrow v_\mathrm{i} > 0,\ v_{\mathrm{i}_0} > 0 \tag{41}$$

$$T < 0 \Rightarrow v_\mathrm{i} < 0,\ v_{\mathrm{i}_0} < 0\,, \tag{42}$$

and, because of that,

$$\frac{v_\mathrm{i}}{v_{\mathrm{i}_0}} \geq 0 \tag{43}$$

is *true in all quadrants*. Thus, for $T < 0$,

$$\boxed{v_{\mathrm{i}_0} = -\sqrt{\frac{|T|}{2\rho A}}\,.} \tag{44}$$

In summary, by including (17), we have

$$\boxed{v_{\mathrm{i}_0} = \mathrm{sgn}(T_\mathrm{n})\sqrt{|T_\mathrm{n}|}\,.} \tag{45}$$

By making use of (32) in conjunction with the functions (30) and (40), we can write the induced velocity v_i as a function of v_r and v_{i_0} for all quadrants:

$$v_\mathrm{i} = \begin{cases} -\frac{v_\mathrm{r}}{2} + \frac{\sqrt{v_\mathrm{r}^2 + 4T_\mathrm{n}}}{2} & \text{for } v_\mathrm{r} > 0,\ T > 0,\ \frac{v_\mathrm{r}}{v_{\mathrm{i}_0}} > 0 \\ & \text{(ahead motion)} \\ -\frac{v_\mathrm{r}}{2} + \frac{\sqrt{v_\mathrm{r}^2 + 4T_\mathrm{n}}}{2} & \text{for } v_\mathrm{r} > 0,\ T < 0,\ \frac{v_\mathrm{r}}{v_{\mathrm{i}_0}} < -2 \\ & \text{(crash-back)} \\ -\frac{v_\mathrm{r}}{2} - \frac{\sqrt{v_\mathrm{r}^2 - 4T_\mathrm{n}}}{2} & \text{for } v_\mathrm{r} < 0,\ T < 0,\ \frac{v_\mathrm{r}}{v_{\mathrm{i}_0}} > 0 \\ & \text{(backward motion)} \\ -\frac{v_\mathrm{r}}{2} - \frac{\sqrt{v_\mathrm{r}^2 - 4T_\mathrm{n}}}{2} & \text{for } v_\mathrm{r} < 0,\ T > 0,\ \frac{v_\mathrm{r}}{v_{\mathrm{i}_0}} < -2 \\ & \text{(crash-ahead)} \end{cases} \tag{46}$$

These expressions are not valid for $\frac{v_\mathrm{r}}{v_{\mathrm{i}_0}} \in [-2, 0]$, the so-called *windmilling region*, in which momentum theory does not hold because of turbulences in the flow that prevent definition of a control volume suitable for momentum theory assumptions (see especially (Leishman, 2006, Sec. 2.13.3)). Leishman describes there the ratio plot as well-defined outside the windmilling state, with a measurement-based curve connecting the well-defined regions of operation. In other words,

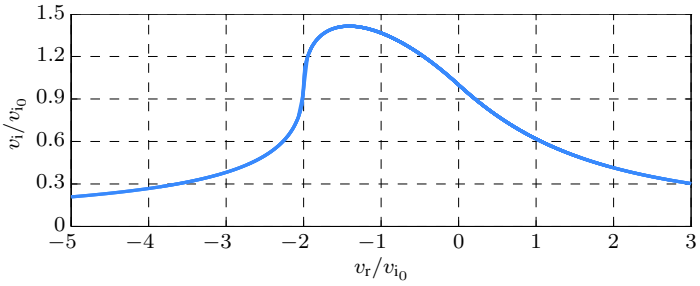

Figure 6: Velocity ratio plot obtained using the odd square and square root functions.

the goal is now to find a formulation of (46) for v_i that allows a closed-form expression as in (45) for v_{i_0}.

To that avail, we developed a new model for the induced velocity, written as

$$\boxed{v_\mathrm{i} = -\frac{v_\mathrm{r}}{2} + \frac{\left(\left(v_\mathrm{r}\right)^{O_2} + 4T_\mathrm{n}\right)^{-O_2}}{2}}\,, \tag{47}$$

where

$$(a)^{\mathrm{O}_2} \text{ is a smoothed version of the } \textit{odd square function } a|a| \text{ with positive slope at zero} \tag{48a}$$

with the *inverse*

$$(a)^{-\mathrm{O}_2} \text{ which is a Lipschitz approximation of the } \textit{odd square root function } \operatorname{sgn}(a)\sqrt{|a|}\,. \tag{48b}$$

By using (47), the induced velocity ratio plot becomes *one* smooth curve that is well-defined on the whole interval of operation, *including* the windmilling state (see Figure 6). It is a remarkable result that, in addition to being $\mathcal{C}^2$-smooth everywhere, the ratio plot has also the same general shape as what is shown in the literature (Leishman, 2006, Fig. 2.18)[1].

Keep in mind that Figure 6 shows numerical results obtained with (47) and (31), respectively, which are the final expressions shaping our development of the momentum theory propeller model. Of special interest here is (Gessow, 1954, p. 3), who writes that because of the division by v_{i_0}, the plot shown in Figure 6 is "independent of disk loading and air density". (Disk loading is the ratio of generated thrust to propeller disk area: DL $= T/A$, see e.g. (Leishman, 2006, p. 71).)

4 PROPELLER MODEL COMPARISON

The momentum theory model is based on idealized assumptions, and it is thus of interest to compare it to other, non-ideal, propeller models in a way that allows for a qualitative statement on the validity of the momentum theory model in relation to the quality of the prognosis we get by using this model.

[1]Published measurements as those in Leishman indicate that, in the windmilling region ($\frac{v_\mathrm{r}}{v_{\mathrm{i}_0}} \in (-2, 0)$), higher values of $\frac{v_\mathrm{i}}{v_{\mathrm{i}_0}}$ may be expected than what is captured by (47). This is where we reach the limits of momentum theory; however, since normal operation of a vehicle does not seek to explore the power generation property of a propeller, the offset can be neglected.

4.1 Instantaneous Power Usage

The instantaneous power usage as defined through momentum theory is

$$P = T(v_\mathrm{r} + v_\mathrm{i})\,, \qquad \text{(31 repeated)}$$

which is known to be the ideal case by definition of the momentum theory model, i.e. all power exerted by the system on the propeller is converted into thrust. The four-quadrant formulation is a non-ideal model, meaning that its *mechanical efficiency*

$$\eta = \frac{Tv}{Q\omega} \tag{49}$$

is less than one. It is therefore the expression in the denominator of (49) that we have to compare with (31). However, for four-quadrant models, $Q\omega$ is a function of v_a and n, rather than v_r and T (which is the case for the momentum theory model), rendering the expressions incomparable in a simultaneous numerical evaluation. Yet, the advance velocity of the four-quadrant model and the relative fluid velocity in the momentum theory model are, by definition, identical; it is only the direction of those velocities in a physical representation of their corresponding models where they differ (cf. Figure 1 and Figure 5a). The other input parameters (n and T, respectively) can be obtained by means of the monotonicity property of the **L**-model: the function $T(n)$, in contrast to its original form, is monotone (see Figure 4) and thus invertible, meaning that n can be expressed as a function of T for a given v_a, thus allowing for a comparison of both models.

The result with respect to propeller performance (Figure 7), is striking: the four-quadrant propeller model requires much more power than the momentum theory propeller model and the achievable thrust with a given power level for a given advance velocity is almost a full order of magnitude smaller than what the same setting can achieve using the momentum theory model.

Another difference, although not of that magnitude, becomes clear by looking at the details of the curves close to the origin: while zero thrust always means zero power requirement for the momentum theory model (i.e., every curve, regardless for what v_r, passes through the origin), this is not true in the four-quadrant model. This reflects the statement earlier made: produced thrust, in reality, goes to zero slightly before the produced torque goes to zero. The power here really *is* a function of torque Q and the propeller's speed of rotation n; therefore we see the effect of P being 0 for values of T that are slightly smaller (or greater) than 0.

4.2 Propeller Efficiency

Finally, it is worthwhile considering a qualitative comparison of all propeller models discussed.

A)Ideal propulsion efficiency: We begin with the momentum theory model and rewrite (27) as

$$T = 2\rho A(v_\mathrm{r} + v_\mathrm{i})v_\mathrm{i} = 2\rho A v_\mathrm{r}^2\left(\frac{v_\mathrm{i}}{v_\mathrm{r}} + \left(\frac{v_\mathrm{i}}{v_\mathrm{r}}\right)^2\right), \tag{50}$$

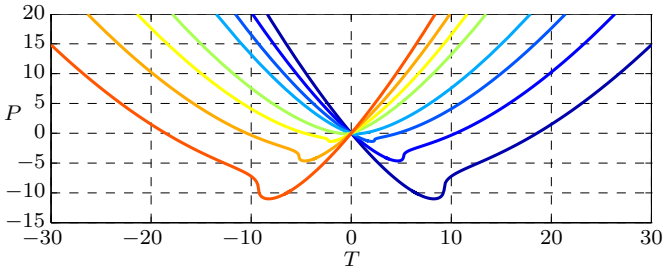

a: Four-quadrant momentum theory model.

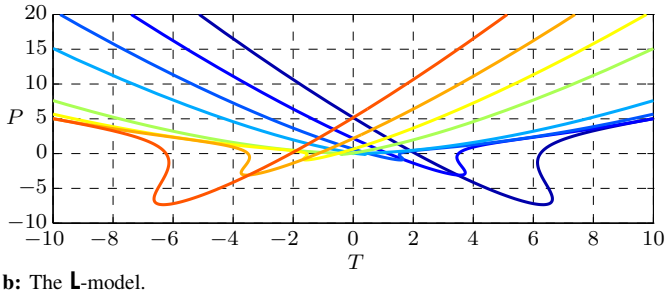

b: The **L**-model.

Figure 7: Power P required to achieve a specified thrust T under the influence of a constant relative fluid velocity v_r (momentum theory) and propeller advance velocity v_a (**L**-model), respectively. The relative fluid velocity ranges from $-2\frac{\mathrm{m}}{\mathrm{s}}$ (blue) to $2\frac{\mathrm{m}}{\mathrm{s}}$ (red) with a gridding of $0.25\frac{\mathrm{m}}{\mathrm{s}}$.

from which we compute that

$$4\left(\frac{v_\mathrm{i}}{v_\mathrm{r}}+\left(\frac{v_\mathrm{i}}{v_\mathrm{r}}\right)^2\right)=\frac{T}{\frac{1}{2}\rho A v_\mathrm{r}^2}=:c_\mathrm{T}^{\mathbf{M}}\,, \tag{51}$$

where $c_\mathrm{T}^{\mathbf{M}}$ is the non-dimensional *momentum theory* thrust coefficient (Clayton and Bishop, 1982, Eq. 7.22). The open-water thrust and torque coefficients k_T and k_Q are given through dimensional analysis and are defined as

$$k_\mathrm{T}:=\frac{T}{\rho n^2 d^4} \tag{52a}$$

$$k_\mathrm{Q}:=\frac{T}{\rho n^2 d^5}\,. \tag{52b}$$

With (52a) and (2), we can derive that

$$\boxed{\frac{k_\mathrm{T}}{J_\mathrm{o}^2}=\left(\frac{T}{\rho n^2 d^4}\right)\left(\frac{n^2 d^2}{v_\mathrm{a}^2}\right)=\frac{\pi}{8}c_\mathrm{T}^{\mathbf{M}}\,.} \tag{53}$$

The ideal efficiency of a propeller is then given by (see (Clayton and Bishop, 1982, Eq. 7.20))

$$\boxed{\eta=\frac{P_\mathrm{out}}{P_\mathrm{in}}=\frac{Tv_\mathrm{r}}{T(v_\mathrm{r}+v_\mathrm{i})}=\frac{2}{1+\left(1+c_\mathrm{T}^{\mathbf{M}}\right)^{1/2}}\,.} \tag{54}$$

Jointly, (54) with (53) allows us to plot the curve $\eta(k_\mathrm{T}/J_\mathrm{o}^2)$ for the momentum theory propeller model.

B)Efficiency of a scaled open-water model: Open-water thrust and torque coefficients were obtained for IST's MEDUSA$_\mathrm{D}$ AUV by scaling a measurement-based model of the MARIUS AUV to match the expected values of thrust and torque at bollard-pull conditions. The exact procedure is out of the scope of this paper; the parameters were determined as

$$k_\mathrm{T}(J_\mathrm{o})=-0.0558J_\mathrm{o}^3+0.1028J_\mathrm{o}^2-0.1819J_\mathrm{o}+0.1951 \tag{55a}$$

$$k_\mathrm{Q}(J_\mathrm{o})=0.0003J_\mathrm{o}^3-0.0095J_\mathrm{o}^2-0.0001J_\mathrm{o}+0.0278 \tag{55b}$$

and are functions of the advance ratio

$$J_\mathrm{o}:=\frac{v_\mathrm{a}}{nD}\,. \qquad \text{(2 repeated)}$$

Using a data gridding on v_r and n, as well as the (mechanical) efficiency (see (Smogeli, 2006, Eq. 2.17))

$$\boxed{\eta=\frac{Tv_\mathrm{r}}{Q\omega}=\frac{J_\mathrm{o}}{2\pi}\frac{k_\mathrm{T}}{k_\mathrm{Q}}\,,} \tag{56}$$

gives the correct expression to be plotted against the ratio $k_\mathrm{T}/J_\mathrm{o}^2$.

C)Four-quadrant efficiency: It is possible to find a mapping of the four-quadrant data into the first-quadrant model (where defined), as e.g. described in (Oosterveld, 1970, p. 42) or (Smogeli, 2006, Sec. 2.1.2): a straightforward calculation gives

$$\tan\beta=\frac{v_\mathrm{a}}{v_\mathrm{p}}=\frac{v_\mathrm{a}}{0.7\pi nd}=\frac{J_\mathrm{o}}{0.7d} \tag{57}$$

and a substitution of (3a) into (52a) results in

$$\begin{aligned}
k_\mathrm{T}&=\frac{T}{\rho n^2 d^4}=\frac{\frac{1}{2}\rho c_\mathrm{T}(\beta)\left(v_\mathrm{a}^2+v_\mathrm{p}^2\right)\pi\left(\frac{d}{2}\right)^2}{\rho n^2 d^4}\\
&=\frac{\pi}{8}c_\mathrm{T}(\beta)\frac{v_\mathrm{a}^2+v_\mathrm{p}^2}{n^2d^2}=\frac{\pi}{8}c_\mathrm{T}(\beta)\frac{v_\mathrm{a}^2+0.7^2R^2\omega^2}{n^2d^2}\\
&=\frac{\pi}{8}c_\mathrm{T}(\beta)\frac{v_\mathrm{a}^2+0.7^2\left(\frac{d}{2}\right)^2 2^2\pi^2n^2}{n^2d^2}\\
&=\frac{\pi}{8}c_\mathrm{T}(\beta)\left(\frac{v_\mathrm{a}^2}{n^2d^2}+0.7^2\pi^2\right)\\
&=\frac{\pi}{8}c_\mathrm{T}(\beta)\left(J_\mathrm{o}^2+0.7^2\pi^2\right)
\end{aligned} \tag{58}$$

In a similar fashion, we combine (3b) and (52b) to obtain

$$k_\mathrm{Q}=\frac{\pi}{8}c_\mathrm{Q}(\beta)\left(J_\mathrm{o}^2+0.7^2\pi^2\right) \tag{59}$$

Then, by substituting the proper terms into (56) as well as the ratio $k_\mathrm{T}/J_\mathrm{o}^2$, we can plot the four-quadrant data in the same manner as done for the other propeller models.

Figure 8 shows the open-water efficiency (first quadrant only) as computed via data gridding on v_r (or v_a in case of the four-quadrant model) and n. This plot gives a unique view over all the propeller models developed in this work, and allows for a qualitative comparison. Furthermore, it shows clearly how, using the simple **L**-model approximation (motivated by the **H**-model approximation), the propeller efficiency curve of a representative thruster captures the main characteristics of the efficiency curve predicted by the models of van Lammeren et al. (1969) and Oosterveld (1970). This plot is seldom shown for small values of $k_\mathrm{T}/J_\mathrm{o}^2$, and it is thus of great interest to see that the efficiency has a peak from which it decreases in both directions—see (Oosterveld, 1970, Fig. 31) for one of the very

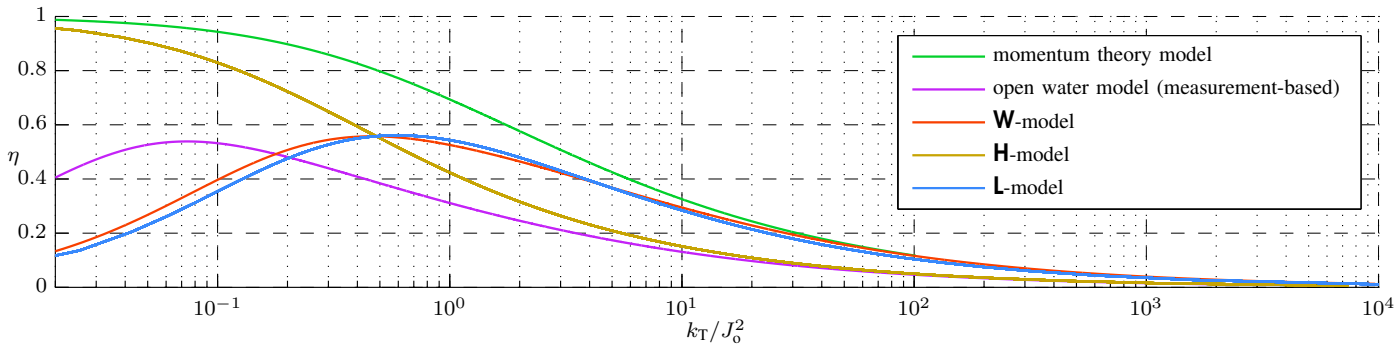

Figure 8: Open-water efficiency η for all propeller models discussed in this work, inspired by Oosterveld (1970) and van Lammeren et al. (1969).

few cases where this is shown in the literature.

5 CONCLUSION

We gave a fast-paced introduction to four-quadrant propeller models and introduced a low-order harmonic approximation that incorporates physical constraints better than another existing approximation. The paper also introduces a novel derivation of the momentum theory propeller model, rendering it applicable in all four quadrants of motion. A comparison between all propeller models shows that our approximation of the standard four-quadrant model, despite being less complex, manages to capture its properties (efficiency and qualitative features of the force and torque curves) closely.

The next steps in our research are the experimental verification of our results and a comparison of the impact of different propeller models in energy-minimal trajectory generation for autonomous underwater vehicles.

ACKNOWLEDGEMENTS

Research supported in part by project MORPH of the EU FP7 (grant agreement no. 288704), and by the FCT Program PEst-OE/EEI/LA0009/2011. The work of A. Häusler (corresponding author) was supported by a Ph.D. scholarship of the FCT under grant number SFRH/BD/68941/2010. Correspondence should be directed to Andreas J. Häusler, ahaeusler@isr.ist.utl.pt.

REFERENCES

Abbott, I.H.A. and von Doenhoff, A.E. (1959). Theory of Wing Sections: Including a Summary of Airfoil Data. Dover Publications, New York.

Anderson, J.D. (1999). Aircraft Performance and Design. WCB/McGraw-Hill, Boston (MA), USA.

Carlton, J. (2007). Marine Propellers and Propulsion. Butterworth-Heinemann, Oxford, 2nd edition.

Clayton, B.R. and Bishop, R.E.D. (1982). Mechanics of Marine Vehicles. Arrowsmith Ltd., Bristol, GB.

Fossen, T.I. (2002). Marine Control Systems: Guidance, Navigation, and Control of Ships, Rigs, and Underwater Vehicles. Marine Cybernetics, Trondheim, Norway.

Gessow, A. (1954). "Review of Information on Induced Flow of a Lifting Rotor: NACA Technical Note 3238". Langley Aeronautical Laboratory, Langley Field (VA), USA.

Hauser, J. (2002). A Projection Operator Approach to the Optimization of Trajectory Functionals. In Proceedings of the 15th IFAC World Congress. Barcelona (Spain).

Häusler, A.J., Saccon, A., Aguiar, A.P., Hauser, J., and Pascoal, A.M. (2012). "Cooperative Motion Planning for Multiple Autonomous Marine Vehicles". In Proceedings of the 9th IFAC Conference on Manoeuvring and Control of Marine Craft (MCMC 2012). Genova, Italy.

Häusler, A.J., Saccon, A., Hauser, J., and Pascoal, A.M. (2013). "Four-Quadrant Propeller Modeling: A Low-Order Harmonic Approximation". In Proceedings of the 9th IFAC Conference on Control Applications in Marine Systems (CAMS 2013). Osaka, Japan.

Healey, A.J., Rock, S.M., Cody, S., Miles, D., and Brown, J.P. (1995). "Toward an Improved Understanding of Thruster Dynamics for Underwater Vehicles". IEEE Journal of Oceanic Engineering, 20, 354–361.

Johnson, W. (1994). Helicopter Theory. Dover Publications, New York, USA, 2 edition.

Leishman, J.G. (2006). Principles of Helicopter Aerodynamics. Cambridge University Press, 2nd edition.

Oosterveld, M.W.C. (1970). Wake Adapted Ducted Propellers. Ph.D. thesis, Delft University of Technology, Wageningen, The Netherlands.

Seddon, J. (1990). Basic Helicopter Aerodynamics. BSP Professional Books, 1st edition.

Sheldal, R.E. and Kilmee, P.C. (1981). "Aerodynamic Characteristics of Seven Symmetrical Airfoil Sections through 180-Degree Angle of Attack for Use in Aerodynamic Analysis of Vertical Axis Wind Turbines". Albuquerque (NM), USA.

Smogeli, Ø.N. (2006). Control of Marine Propellers: From Normal to Extreme Conditions. Ph.D. thesis, Norwegian University of Science and Technology (NTNU), Trondheim, Norway.

van Lammeren, W.P.A., van Manen, J.D., and Oosterveld, M.W.C. (1969). "The Wageningen B-Screw Series". Transactions of SNAME, 77, 269–317.